Utilization of Coinage Metals as an Efficient Dopant Protocol for Enhancing Asymmetric Supercapacitors and Oxygen Evolution Reactions

Ambedker Meghwar, Ahmed Raza, Haresh Kumar, Jethanand Parmar, Wanhinyal Dars, Rameez Mangi, Masroor Ali Bhellar, Fida Hussain, Ghansham Das, Kashif Ali, et al.

Utilization of coinage metals as an efficient dopant protocol for enhancing asymmetric supercapacitors and oxygen evolution reactions

Ambedker[a], Ahmed Raza[a], Haresh Kumar[a], Jethanand[a], Wanhinyal[a], Rameez Mangi[a], Masroor Ali Bhellar[a], Fida Hussain[a], Ghansham Das[a], Kashif Ali[a], Aneela Tahira[c], Muhammad Ali Bhatti[f], Elmuez Dawi[d], Rafat M. Ibrahim[e], Brigitte Vigolo[b], Jawaid Ali Lighari[f], Zafar Hussain Ibupoto[a*]

[a]*Institute of Chemistry, University of Sindh Jamshoro, 76080, Sindh, Pakistan.*

[b]*University de Lorraine, CNRS, IJL, F-54000 Nancy, France.*

[c]*Institute of Chemistry, Shah Abdul Latif University Khairpur Mirs, Sindh, Pakistan.*

[d]*College of Humanities and Sciences, Mathematics and Science department, Ajman University, P.O.Box 346, Ajman, UAE.*

[e]*Physics Department, Faculty of Science, Taibah University, Al- Madaina Al Munawarah 42353, Saudi Arabia*

[f]*Centre for Environmental Sciences, University of Sindh Jamshoro, 76080, Sindh, Pakistan.*

[*]*Corresponding author(s):*

Zafar Hussain Ibupoto, PhD, Email : zaffar.ibhupoto@usindh.edu.pk

Abstract

Doped polyaniline (PANI) was synthesized using low concentrations of Ag and Cu coinage metals in order to evaluate their impact on energy conversion and storage performances. During the preparation of PANI, a chemical oxidation polymerization process was followed by concurrent doping with Ag and Cu. The nanoparticles were found to have typical orientations when examined by scanning electron microscopy (SEM). X-ray diffraction (XRD) was used to examine the crystal structure of the synthesized doped PANI materials, which confirmed their crystalline nature. Ag-Cu-doped PANI samples demonstrated a more pronounced reduction in optical band gap as compared to other doped samples. Based on Fourier transform infrared spectroscopy (FTIR) analysis, it can be concluded that the synthesized materials possess large

functional groups. Compared to other enhanced PANI materials in an alkaline electrolyte, Ag-Cu enriched PANI exhibited superior oxygen evolution reaction (OER) and supercapacitor performances. The presence of the oxygen evolution reaction activity (OER) in a 1M KOH solution was observed at an overpotential of 340 mV at a current density of 10 mA/cm^2. Using Ag-Cu doped PANI as the anode electrode material, asymmetric supercapacitors produced energy density of 211.75 Wh/kg at a current density of 4.5 A/g, demonstrating their superior performance. The obtained results described high cycle stability over 50000 galvanic charge-discharge cycles at a current density of 4.5 A/g and a 102% capacitance retention rate was described by the electrode material. Despite low concentrations of Ag and Cu dopants, the coinage metals can be effectively used as dopants for the fabrication of next-generation practical energy storage devices.

Keywords: Polyaniline, Silver and Copper, Oxygen evolution reaction, Asymmetric supercapacitor.

Graphical abstract

An expression of the simultaneous synthesis of doping Ag-Cu into PANI with a view to enhancing the electrochemical performance in asymmetric supercapacitors as well as oxygen evolution reactions.

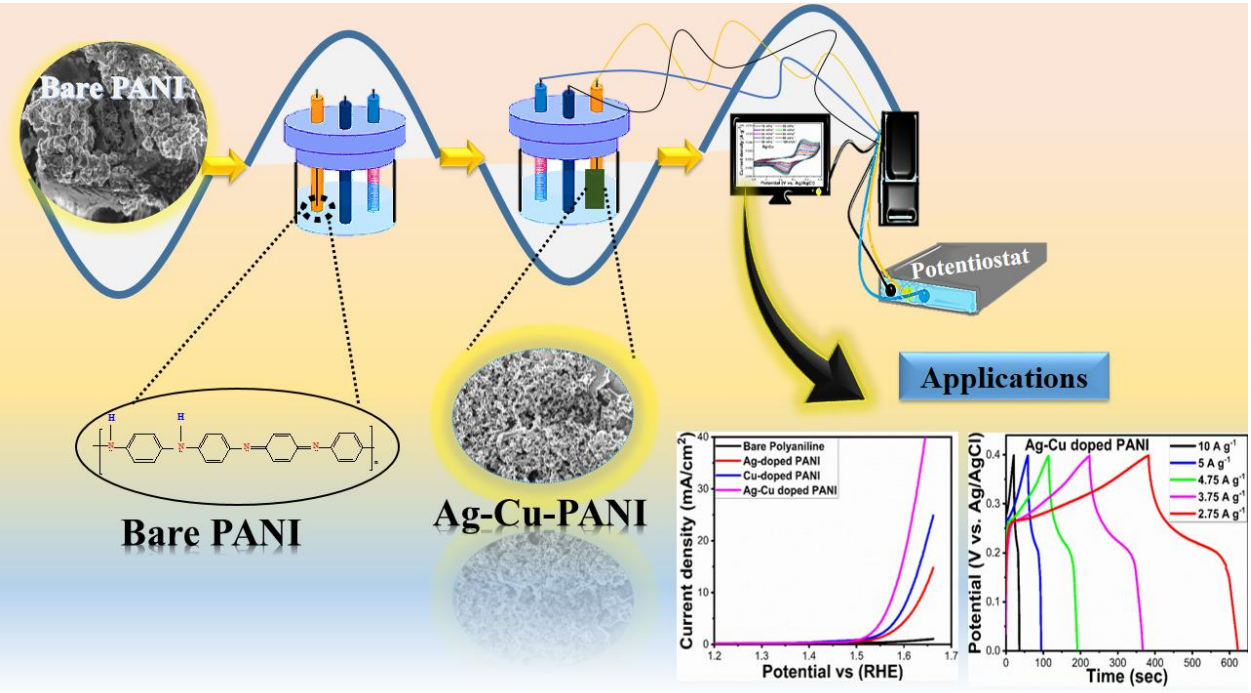

1. Introduction

Hydrogen, recognized for its high energy density, is considered one of the most critical energy sources [1]. Fuel cell vehicles use hydrogen to generate electricity and power without emitting greenhouse gases. Traditional methods of hydrogen production, such as coal gasification, steam reforming, plasma reforming, and pyrolysis of natural gases, result in brown or grey hydrogen with carbon dioxide emissions [2]. These methods can be integrated with carbon dioxide capture technology to produce blue hydrogen [3, 4]. For sustainable hydrogen energy utilization, developing effective methods to generate green hydrogen using renewable resources is essential. Solar-driven hydrogen production and electrolysis are potential processes for green hydrogen production, although the cost of these technologies is significantly higher than fossil fuel sources [5, 6, 7]. The water splitting process, which involves the oxygen evolution reaction (OER) at the anode and the hydrogen evolution reaction (HER) at the cathode, is crucial for hydrogen production [8, 9]. The OER process, due to its four-electron transfer and high energy input, is kinetically slower than the HER process. To address this, electrocatalysts have been designed to

facilitate OER at lower energy levels. Current state-of-the-art electrocatalysts for OER include noble metals like ruthenium (Ru) and iridium (Ir); however, their scarcity and high cost limit their commercial viability [10, 11]. There is an urgent need for efficient, earth-abundant electrocatalysts to advance green hydrogen production through water splitting. Renewable energy sources, with their attractive features, necessitate energy storage devices capable of harvesting, storing, and utilizing energy as needed [12]. Researchers have focused on developing energy storage and conversion systems such as supercapacitors, batteries, and fuel cells [13]. Supercapacitors are particularly notable for their high power density, excellent cycling stability, rapid charge and discharge rates, and low maintenance costs [14, 15]. Their performance lies between conventional capacitors and batteries, making them suitable for various applications, including memory backup devices, hybrid electric vehicles, and power grids [16].

Supercapacitors typically consist of a cathode, anode, separator, and electrolyte, with the electrode being a critical component. The performance of electrodes in supercapacitors depends on their electrochemistry of power storage systems such as microstructure, surface area, and porosity [17]. Electrodes with large surface areas and numerous redox active sites enhance electrochemical activity. In contrast, those with high porosity improve cycling stability by reducing strain during long charging and discharging cycles [18]. The interface between electrode and electrolyte also significantly impacts supercapacitor performance [14].

Material engineers and scientists prioritize electrode materials design, focusing on high specific capacitance, excellent cycling stability, and robust mechanical and structural stability [19]. Conducting polymers, carbonaceous materials, metal nitrides, and metal oxides have been employed in supercapacitor development [20]. Conducting polymers, such as polyparaphenylene (PPP), polyacetylene (PA), polythiophene (PT), poly(3,4-ethylenedioxythiophene) (PEDOT), polypyrrole (PPy), and polyaniline (PANI), are favored for their electrical conductivity, light weight, ease of synthesis, and low cost [20, 21]. Polyaniline (PANI) has been extensively researched due to its high specific theoretical capacitance, electrical conductivity, high energy density, electrochemical stability, and redox activity [22]. However, its poor structural and mechanical stability limits its use as an electrode material, as it exhibits volumetric instability and capacitance deterioration during repeated charging and discharging cycles. Pure PANI degrades above 50% capacitance retention after 1000 cycles [23]. To address this, PANI has

been integrated with metal oxides, resulting in improved cycling stability through a synergistic effect [24]. PANI has been considered with transition metal oxides due to their high power and energy density during supercapacitors development. Transition metal oxides, including NiO, Fe_2O_3, V_2O_5, RuO_2, Co_3O_4, TiO_2, MnO_2, and Nb_2O_5, have been used with PANI to enhance supercapacitor performance [25]. Compared to their separate counterparts, composite electrode materials composed of conducting polymers and transition metal oxides demonstrate enhanced electrochemical activity [26]. PANI is synthesized using dopants like sulfonic acid and HCl acid, producing highly ordered crystals [24]. PANI's electronic properties can be tuned by doping with transition metals, which generate polarization on the chain, acting as ionic conductors and charge carriers [27]. Doping PANI with transition metals such as Ag^+ and Fe^{3+} enhances supercapacitor performance by increasing surface area and electrical conductivity. Similarly, doping PANI with copper has increased electrochemical activity [28]. Separate studies have been carried out for evaluating the impact of Ag and Cu on the performance of PANI, however there is no study in the existing literature dealing with the simultaneous doping of Ag and Cu into PANI during chemical oxidative polymerization.

The combination of silver (Ag) and copper (Cu) dopants in polyaniline with a finite quantities for enhanced oxygen evolution reaction (OER) and asymmetric device applications has not been previously investigated. Ag and Cu have been found to promote charge transport rates, surface area, and catalytic sites. Therefore, they are expected to provide excellent electrocatalysts for asymmetric devices and electrode materials. Ag and Cu doped into polyaniline for enhanced OER and asymmetric device applications have not previously been investigated. It has been demonstrated for the first time that Ag and Cu dopants together can improve the polyaniline based electrode material for energy conversion and storage device applications.

2. Materials and Methods

2.1.Chemical reagents

Sigma Aldrich Karachi, Sindh Pakistan provided a variety of high analytical grade materials, including nickel foam, copper nitrate dihydrate, aniline ($C_6H_6NH_2$), silver nitrate, hydrochloric acid, potassium persulfate ($K_2S_2O_8$), potassium hydroxide, ethanol, and sulfuric acid (H_2SO_4). Aniline underwent a double distillation process before being synthesized.

2.2.Synthesis of Ag-Cu doped PANI composites using chemical oxidation process

A variety of samples were prepared, including bare PANI, Ag-doped PANI, Cu-doped PANI, and Ag-Cu-doped PANI. An aniline solution 0.1 M in 0.1M HCl was prepared in one beaker, and potassium persulfate ($K_2S_2O_8$) solution 0.1 M in 0.1M HCl was prepared in another beaker. A beaker containing 0.1 M of aniline was then slowly added drop-by-drop with 0.1 M $K_2S_2O_8$, resulting in a dark color. The final observation was the appearance of dark green precipitates of PANI. PANI precipitates were allowed to settle at the bottom of the beaker after the solution settled. The solution was filtered after six hours in order to collect the precipitates, which were washed several times using deionized water and absolute ethanol. For the preparation of Ag doped APNI, the same procedure as for PANI was followed, except that 0.3 mM silver nitrate was added dropwise to 0.1 M aniline solution in 0.1 M HCl, followed by 0.1 M potassium persulfate in 0.1 M HCl. Similar to the Ag doped PANI, the Cu doped PANI was fabricated using 0.3mM copper nitrate dihydrate. The Ag-Cu doped PANI was synthesized by adding 0.3 mM silver nitrate and 0.3 mM copper nitrate dihydrate to PANI simultaneously, resulting in a dark green colored Ag-Cu doped PANI. Following the collection of the above materials, they were allowed to dry overnight at 65 °C, and then structural and electrochemical analyses were conducted.

2.3.Structural characterization

The shape of bare PANI and doped PANI materials was studied using a field emission scanning electron microscope (Zeiss GeminiSEM 500). As-synthesized materials were evaluated using powder X-ray diffraction (PXRD), X-ray spectroscopy, UV-visible spectroscopy, and Fourier transform infrared spectroscopy, applied on KBR disk, were used to examine optical properties, and Fourier transform infrared spectroscopy was employed to determine functional groups.

2.4.Electrode fabrication using Ag-Cu doped PANI for various electrochemical tests

Separate beakers were used to disperse the electrode materials in a mixture of ethanol and water containing 5 mg of electrode materials along with 5% Nafion. An ultrasonic bath was used to obtain a homogenous slurry over a period of 20 minutes. A 2x2 cm^2 piece of nickel foam was then taken and washed several times with 2M HCl solution, followed by ethanol and distilled

water. After drying, the electrode material was dipped five to nine times in the slurry of electrode materials prepared above. Following sintered electrodes, the electrochemical performance of the electrodes was evaluated at 60 ºC for 20 minutes. The electrodes were loaded with a mass of 0.2 mg each. Under the conditions of 100 kHz to 0.1Hz, an amplitude of 5 mV and biasing the OER onset potential, several electrochemical modes were conducted, including linear sweep voltammetry (LSV), cyclic voltammetry (CV), chronoamperometry, galvanic charge-discharge (GCD) and electrochemical impedance spectroscopy. Under the given equations 1-3, the specific capacitance, energy density, and power density were calculated.

$$C = I \times \Delta t/\Delta V \times m \quad (1)$$

$$E = [C \times (\Delta V)^2]/7.2 \quad (2)$$

$$P = [E \times (\Delta t)]/3.6 \quad (3)$$

3. Results and Discussion

3.1. Morphology, crystal structure, optical and functional group analysis of as synthesized PANI

Based on SEM analysis, pure PANI exhibits an indefinite form that is typical of polymers (Figure 1a). Despite the doping with Ag, Cu, or both (Figure 1b, 1c, and 1d, respectively), the morphological aspect of the doped-PANI materials remains quite similar to that observed for pure PANI, possibly due to the low concentrations of the used dopants. In contrast, Ag-Cu-doped PANI shows a much greater porosity (Figure 1d). By powder XRD, Figure 2 illustrates the diffraction patterns of Ag-doped PANI, Cu-doped PANI, Ag-Cu-doped PANI, and bare PANI. Compared to the bare PANI all the doped samples show more intense and pronounced peaks at 25.3°, with shoulder reflections occurring at 21.2° and 14.1°, corresponding to Miller indices of (200), (020), and (011), respectively. On the basis of these patterns, it appears that chemical oxidation polymerization has been successful in preparing PANI. XRD patterns of coinage

metallic ion-doped PANI were similar to those of bare PANI, indicating that the ions were present without altering the crystal structure.

According to Figure 3a-c, FTIR analysis of coinage metallic ion-doped PANI provides information regarding chemical bonds. An IR spectrum of bare PANI was observed at 1600 and 1480 cm^{-1}, attributed to the quinone structure and the C=C stretching frequency of the benzene molecule. It is believed that the IR band around 1300 cm^{-1} is a consequence of C-N stretching. Observations of C-H bending vibrations in plane and out of plane were made at 1140 and 817 cm^{-1}, respectively. FTIR spectra of metal ion dopants in PANI showed similar shifts in the IR bands, suggesting that these dopants interact with PANI's covalent bonds. Following successful doping with coinage metallic ions, an FTIR analysis indicated that the structural characteristics of PANI had been retained.

The UV-VIS spectra of bare PANI, Ag-doped PANI, Cu-doped PANI, and Ag-Cu-doped PANI are shown in Figures 4a-d. We found a characteristic band around 364 nm, which indicated the π-π transition of the benzenoid structure of PANI. However, metallic ion dopants from coinage showed a hypsochromic shift, indicating a strong interaction with PANI. Tauc's plots were used to calculate the optical band gap as shown in the inset of Figure 4a-d. The optical band gaps of PANI, Ag-doped PANI, Cu-doped PANI, and Ag-Cu-doped PANI are 2.72 eV, 4.48 eV, 2.44 eV, and 2.35 eV, respectively. Coinage metallic ion doping may allow shallow states within the optical band gap, resulting in a decrease in optical band energy.

3.2. Electrocatalytic activity of as synthesized coinage metals doped PANI

As synthesized electrocatalysts, bare PANI, Ag-doped PANI, Cu-doped PANI, and Ag-Cu doped PANI were evaluated using linear sweep voltammetry (LSV) at 2 mV/s in 1.0 M KOH electrolyte. The assembly of this cell was based on the use of three electrodes. As shown in Figure 5a, Ag-Cu doped PANI displays superior OER activity in terms of low onset potential and overpotential in comparison to bare PANI, Ag-doped PANI, and Cu-doped PANI, indicating the synergetic impact of Ag and Cu on the synthesized Ag-Cu doped PANI material, which has improved the catalytic sites, charge transport, and redox activity. In our study, we determined the overpotentials of Ag-doped PANI, Cu-doped PANI, and Ag-Cu doped PANI at 10 mA/cm^2 as 410 mV, 380 mV, and 340 mV respectively, as shown in Figure 5b. The enhanced

electrochemical activity of PANI can be attributed to the fast charge transfer rate, improved redox activity, catalytic centers, and modified surface of the material caused by doping Ag and Cu. The synergetic effect of both coinage metals and PANI's structure resulted in a significant reduction in overpotential, resulting in excellent OER. As shown in Figure 5c, Tafel curves were fitted to the Tafel equation in order to evaluate the kinetics of OER. Tafel values of Ag-Cu doped PANI were relatively smaller than those of bare PANI, Ag-doped PANI, and Cu-doped PANI, with values of 126 mV/dec, 105 mV/dec, and 93 mV/dec, respectively. Due to the large surface area of Ag-Cu doped PANI, the fast charge transfer rate, and the modified surface, high density of reactive species such as H_2O, OH^{-1}, and others was facilitated during the OER process. As a result, Ag-Cu doped PANI demonstrated a faster OER kinetic than the other electrocatalysts shown in Figure 5c. In order to determine the enhanced rate of interfacial charge transfer, an electrochemical impedance spectroscopy experiment was conducted. For the Nyquist plots, an equivalent circuit with well-defined circuit elements, such as solution resistance (Rs), charge transfer resistance (Rct), and capacitance double layer (Cdl), is shown in Figure 5d. As compared to bare PANI, Ag-doped PANI, and Cu-doped PANI, Ag-Cu doped PANI exhibits the smallest semicircle arc, indicating that this electrocatalyst exhibits the least charge transfer resistance. In the case of bare PANI, Ag-doped PANI, Cu-doped PANI, and Ag-Cu doped PANI, the measured charge transfer resistance was 57.89 Ohm, 18.43 Ohm, 7.85 Ohm, and 3.79 Ohm, respectively. It is possible that the synergetic effect of Ag-Cu doping within the interfacial chemistry of the PANI may have enhanced the PANI's electrical conductivity.

Water electrolysis is characterized by surface reactions followed by adsorption and desorption of reactive species on the electrocatalyst surface. Due to this, the estimation of the surface active sites is of utmost importance. A sample of as-synthesized material was subjected to non-faradic cyclic voltammetry (CV) measurements at varying scan rates, and their corresponding CV curves are shown in Supplementary Figure (S1). An electrocatalyst containing Ag-Cu was tested at a fixed current density using chronoamperometry, as shown in Figure 5e. It has been observed that the electrocatalyst has a high tendency to retain the overpotential at fixed current density without any potential drop, demonstrating outstanding durability that can be attributed to the modified surface area and porosity of the electrode, which made it possible for gaseous species to flow through easily. The stability of Ag-Cu doped PANI was evaluated by measuring the LSV curves before and after the durability test, as shown in Figure 5f. It is important to note that the Ag-Cu

doped PANI exhibits negligible shifts in onset potential and almost maintains the overpotential without any loss in current density, thereby demonstrating significant stability. According to the results of the durability and stability tests, Ag-Cu doped PANI may be used as an alternative electrocatalyst for electrochemical water splitting. Ag-Cu doped PANI could provide the multi catalytic centers for the adsorption of hydroxide ions, tunable charge transport, and facilitation of charge transfer at the electrode and electrolyte interfaces, modified surface properties and increased mechanical stability for the PANI structure through the induction of coinage metallic ions as dopant. The performance of OER activity was compared with the recent fabricated electrocatalysts as given in Supplementary Table (S1). It could be viewed that the proposed Ag-Cu doped PANI material has superior or equal performance to many of the recent electrocatalytic materials in the alkaline media.

3.2. Supercapacitor application of coinage metals doped PANI

A cyclic voltammetry (CV) and galvanic charge-discharge electrochemical method was used to evaluate the performance of bare nickel foam, PANI, Ag doped PANI, Cu doped PANI, and Ag-Cu doped PANI composites in 3.0M KOH electrolytic solution. For the CV measurements, we used a three electrode cell set up to determine the pseudocapacitance of the synthesized electrode materials. A series of scan rates from 10 mV/s to 100 mV/s was taken into consideration within the potential window of 0 -0.6V against Ag/AgCl. As shown in Figure 6, the area under CV curves increased linearly with scan rate due to the excellent electrochemical properties of coinage metal doped PANI that support the redox behavior of electrode materials. In the aqueous electrolytic solution, these observations confirm the distinctive electrochemical kinetics of the electrode materials presented. The high surface area, fast charge transfer rate, and modified surface of PANI might account for this attribution of high performance [34, 35, 36]. There is no doubt that the CV curves demonstrate obvious redox peaks suggesting successive faradic reactions with enhanced charge transfer rates. Compared to bare nickel foam and PANI, Ag doped PANI, Cu doped APNI, and Ag-Cu doped PANI significantly improved the redox peaks current. However, Ag-Cu PANI presented the highest redox characteristics as a result of the synergetic effect of simultaneous doping of Ag and Cu, which altered the surface properties of the electrode. In order to gain a deeper understanding of the charge storage mechanisms within the synthesized electrode materials, we examined the contributions of capacitive and diffusion-controlled aspects using CV curves at different scan rates in accordance with equation [37]:

$$i_p = k_1 v + k_2 v^{1/2} \quad (4)$$

Here, K1 as slope and K2 as intercept being constant estimated from the linear correlation between $i/v^{1/2}$ *vs.* $v^{1/2}$.

In Figure 6a-d, the relative quantitative values of K1 and K2 illustrate the contribution of capacitive and diffusion-controlled charge storage mechanisms to each electrode material could be calculated. According to Figure 7a-d, the relative contributions of capacitive and diffusion-controlled processes can be determined using the estimated K1 and K2.

The estimated contributions of capacitive and diffusion-controlled effects are presented in Figure 7a-d for bare PANI, Ag doped PANI, Cu doped PANI, and Ag-Cu doped PANI. At slower scan rates, diffusion-controlled faradic processes dominate because electrolytic ions have sufficient time to penetrate into the electrode material and participate in the charge transfer process. As shown in Figure 8a-d, increasing the scan rate improves the surface-controlled interfacial capacitance contribution. For all of the electrode materials tested, it is evident from these CV analyses that the capacitive contribution gradually increases with increasing scan rates. It is possible that Ag-Cu doped PANI would exhibit improved capacitive contributions as a result of the synergetic effect of Ag and Cu being simultaneously incorporated into PANI, thus modifying the surface and improving the efficiency of the charge transfer. Furthermore, GCD electrochemical mode was applied to all electrode materials presented at varying current densities and with potential windows ranging from 0 to 400. Each electrode material was tested at the same set of varied current densities. In Figure 9a-e, the GCD curves demonstrate typical pseudocapacitor behavior with nonlinear characteristics. In accordance with the measurements of CV curves, the behaviors of each electrode material are highly consistent with GCD curves, which is consistent with the pseudocapacitive properties of polyaniline as an electrode material. Specific capacitance was calculated from GCD curves at different current densities using Equation 1. At fixed current densities, the specific capacitances of bare PANI, Ag doped PANI, Cu doped PANI, and Ag-Cu doped PANI 2.75, 3.75, 4.75, 5, and 10 F/g , respectively.

Figure 9f shows the specific calculations for each electrode material at different current densities. As a result of its high surface area, significant electroactive sites for redox reactions, fast charge transfer kinetics, and high adsorption of electrolytic ions, Ag-Cu doped PANI exhibited the greatest specific capacitance, which resulted in better charge storage. An analysis

of the electrochemical properties of different polyaniline-based composite electrode materials is presented in Supplementary Table (S1). As demonstrated by the relative specific capacitance of the present electrode material with that of the previous electrode materials, it is capable of storing a greater amount of energy than the previous electrode materials. Several factors contribute to the superior charge storage properties of Ag-Cu doped PANI electrode materials, including rapid charge transfer kinetics through simultaneous doping of Ag and Cu, as well as modified surfaces which are able to adsorb large amounts of electrolytic ions using doping precursors. Dopants added to PANI enhanced the penetration of electrolytic ions inside the electrode material, thus enhancing charge diffusion and improving charge storage efficiency. The brief summary of estimated results from GCD curves at various current densities for the three electrode are given in Supplementary Table (S2).

3.3. Asymmetric device fabrication based on Ag-Cu doped PANI electrode material

Two-electrode asymmetric supercapacitors (ASCs) were manufactured using rice husk-derived activated carbon (AC) as the cathode and Ag-Cu doped PANI as the anode. According to Supplementary Figure (S1), the CV curves of AC showed negligible farad properties at different scan rates. An electrolytic solution containing 3.0M KOH was applied to the cathode and anode electrodes. Figure 10a illustrates CV versus Ag/AgCl within a potential window of 0 to 1.6 V. The scan rate was varied from 10 mV/s to 150 mV/s. A typical rectangular pattern was evident in the CV curves at different scan rates, which indicates that the cell is set up to exhibit pseudo-capacitive behavior. Although the scan rate was varied, CV curves remained unchanged, demonstrating ASC's excellent reversibility and redox performance. In Figure 10b, the GCD profiles are depicted at various current densities using a potential window of 0 to 1.6 V. Equation 1 is used to calculate specific capacitance based on the GCD curves at different current densities. As for the ASC, the highest specific capacitance of 211 F/g was found at the lowest current density of 4.5 A/g, as depicted in Figure 10c. As shown in Figure 10d illustrates the calculated power and energy densities at different current densities. By using coinage metals as dopants, the polyaniline was able to store energy at 4.5 A/g with enhanced performance. Possibly, this is due to the unique architecture, rapid charge transfer kinetics, and large surface area of the Ag-Cu doped PANI anode electrode. For the purpose of evaluating the cycling stability of the ASC device in terms of percentage capacitance retention, 50,000 repeatable GCD cycles were performed at a constant current density of 4.5 A/g at constant voltage to determine the cycling

stability of the device. Figure 10e illustrates the use of repeatable 50,000 GCD cycles for estimating the coulombic efficiency. As can be seen from the figure, a remarkable % of capacitance was retained, and a coulombic efficiency of 87.9% was achieved. In addition the enhanced charge transfer rate between the presented electrode material and electrolyte, numerous energy storage sites are present within Ag-Cu doped PANI resulting in the significant improvement in cycling stability of ASC [38]. These properties of the electrode material enable the device to store and release energy in repeatable cycles, resulting in improved capacitance. In a variety of applications, this excellent cycling stability confirms the promising, reliable, and long-term use of Ag-Cu doped PANI electrode material. A summary of obtained results is shown in Table 1. The electrochemical double layer capacitance (Cdl) was used to estimate the electrochemical active surface area (ECSA). The non-faradic CV curves of bare PANI, Ag doped PANI, Cu doped PANI and Ag-Cu doped PANI were recorded at different scan rates as shown in Supplementary Figure (S2). The Cdl values in Figure 10f are derived from the slope of the linear fit of the difference between anodic and cathodic side currents of CV curves at sweeping scan rates and divided by 2. Among PANI materials, the Cdl values were 8.17 $mFcm^{-2}$ in the bare PANI, 10.36 $mFcm^{-2}$ in the Ag doped PANI, 11.52 $mFcm^{-2}$ in the Cu doped PANI and 12.19$mFcm^{-2}$ in the Ag-Cu doped PANI, respectively. Due to the simultaneous doping of Ag and Cu, the surface of PANI was clearly modified, resulting in the highest active ECSA value. The charge storage performance of Ag-Cu doped PANI was highly enhanced owing to its modified surface for the rapid rate of adsorption of hydroxide ions, fast charge transfer rate, improved mechanical stability of molecular structure of PANI, and increased solubility of doped PANI, consequently an excellent electrochemical performance was demonstrated. The comparative analysis of ASC device was done with the reported ASC devices as given in Supplementary Table (S3). It was noticed that the proposed ASC device has superior specific capacitance, energy density and power density.

4. Conclusions

We synthesized coinage metal-doped polyaniline using chemical oxidative polymerization method. Coinage metals such as Ag, Cu were used as dopants in PANI. A variety of

spectroscopic techniques have been used to study the shape, size, crystallinity, chemical composition, and optical properties of the doped PANI, including SEM, XPS, XRD, FTIR, and UV-visible spectroscopy. As a result of adding coinage metals like Ag and Cu to PANI, a nanoparticle-like morphology was observed in PANI. Among the doped PANI samples, the Ag-Cu doped sample was found to be the most efficient for both OER and asymmetric supercapacitors. A low overpotential of 340 mV was observed for Ag-Cu doped PANI at 10 mA/cm^2. PANI composites doped with Ag-Cu exhibit excellent pseudocapacitance properties, making them suitable for asymmetric supercapacitors. The specific capacitance of the ASC device is 642.86 F/g, the energy density is 211.75 Wh/kg, and the power density is 3465.0 W/kg at a fixed current density of 4.5 A/g. Further, the electrode material demonstrated outstanding cycling stability during 50,000 repeatable GCD cycles at a current density of 4.5 A/g, with a retention capacitance of 102%. The high performance of Ag-Cu doped PANI may be explained by the modification of the surface, the rapid charge transfer kinetics, and the synergetic effect of simultaneous doping with Ag and Cu coinage metals. Based on these electrochemical performance perspectives, coinage metals such as Ag and Cu could be considered potential dopants for the development of next-generation electrode materials for energy storage and conversion.

Acknowledgments

Authors would also like to acknowledge the partial funding of the Ajman University, Grant ID: DRG ref. 2024-IRG-HBS-01. Brigitte Vigolo would like to thank the platform “Microscopies, Microprobes and Metallography (3M)” (Institut Jean Lamour, IJL, Nancy, France).

Conflicts of Interest: Authors have no conflict of interest in the presented research work.

Data Availability Statement: The authors declare that the data supporting this study's findings are available within the paper.

5. References

1. J. Wang, “Reconstructing oxygen electrocatalysts for hydrogen energy applications,” *Current Opinion in Electrochemistry*, **39** (2023): 101304.
2. M. Younas, S. Shafique, A. Hafeez, F. Javed, and F. Rehman, "An overview of hydrogen production: current status, potential, and challenges,” Fuel. 316 (2022): 123317.
3. J. Incer-Valverde, A. Korayem, G. Tsatsaronis, and T. Morosuk, “Colors” of hydrogen: Definitions and carbon intensity,” Energ. Conver. Manage.,**291** (2023): 117294.
4. A. Ajanovic, M. Sayer, and R. Haas, “The economics and the environmental benignity of different colors of hydrogen,” Int. J. Hydrogen Energy, **47** (2022): 24136-24154.
5. L. Chen, J.T. Ren, and Z.Y. Yuan, “Design strategies of phosphorus-containing catalysts for photocatalytic, photoelectrochemical and electrocatalytic water splitting,” Green Chem., **24** (2022): 713-747
6. F. Zhang, and Q. Wang, “Redox-mediated electrocatalytic and photocatalytic hydrogen production,” Curr. Opin. Electrochem., **35** (2022): 101097.
7. B. Panigrahy, K. Narayan, and B.R. Rao, “Green hydrogen production by water electrolysis: a renewable energy perspective,” Mater. Today:. Proc., **67** (2022): 1310-1314.
8. K.E. Ramohlola, M.J. Hato, G.R. Monama, E. Makhado, E.I. Iwuoha, and K.D. Modibane, “State-of-the-art advances and perspectives for electrocatalysis,” Methods Electrocatal.: Adv. Mater. Allied Appl. (2020): 311–352.
9. K.E. Ramohlola, T.C. Morudu, T.C. Maponya, G.R. Monama, E. Makhado, P.S. Ramaripa, M.J. Hato, E.I. Iwouha, A. Khan, and K.D. Modibane, “Metal-organic frameworks with immobilized nanoparticles for hydrogen generation,” in: Metal-Organic Framework Nanocomposites (2020): 291-332. CRC Press.
10. M.V. Pagliaro, M. Bellini, F. Bartoli, J. Filippi, A. Marchionni, C. Castello, W. Oberhauser, L. Poggini, B. Cortigiani, L. Capozzoli, and A. Lavacchi, “Probing the effect of metal-CeO2 interactions in carbon supported electrocatalysts on alkaline hydrogen oxidation and evolution reactions,” Inorg. Chim. Acta, **543** (2022): 121161.
11. Y. Liu, Q. Wang, J. Zhang, J. Ding, Y. Cheng, T. Wang, J. Li, F. Hu, H.B. Yang, and B. Liu, “Recent advances in carbon-supported noble-metal electrocatalysts for hydrogen evolution reaction: syntheses, structures, and properties,” Adv. Energy Mater., **12** (2022): 2200928.

12. P.E. Lokhande, U.S. Chavan, and A. Pandey, "Materials and fabrication methods for electrochemical supercapacitors: overview," Electrochem. Energy Rev., **3** (2020): 155-186.
13. A.A.Z. Diab, H.M. Sultan, and O.N. Kuznetsov, "Optimal sizing of hybrid solar/wind/hydroelectric pumped storage energy system in Egypt based on different meta-heuristic techniques," Environ. Sci. Pollut. Res., **27** (2020): 32318-32340.
14. A. Muzaffar, M.B. Ahamed, K. Deshmukh, and J. Thirumalai, "A review on recent advances in hybrid supercapacitors: Design, fabrication and applications," Renew. Sustain. Energy Rev., **101** (2019): 123-145.
15. M.H. Boratto, J.V. Lima, G.G. Malliaras, and C.F. Graeff, "Supercapacitor auto analyser: An automated data analysis software for supercapacitor characterization," J. Energy Storage, **63** (2023): 107095.
16. J. Sun, C. Xu, H. Chen, "A review on the synthesis of CuCo2O4-based electrode materials and their applications in supercapacitors," J. Mater., **7** (2021): 98-126.
17. H. Sun, Y. Miao, G. Wang, X. Han, C. Xu, J. Zhu, and H. Chen, "Battery-type ZnCo2O4 nanosheets and nanowires as advanced cathode materials for hybrid supercapacitors with ultra-long cycling stability," J. Energy Storage, **92** (2024): 112189.
18. Y. Wu, and C. Cao, "The way to improve the energy density of supercapacitors: Progress and perspective," Sci. China Mater., **61** (2018): 1517-1526.
19. M.M. Sk, C.Y. Yue, K. Ghosh, and R.K. Jena, "Review on advances in porous nanostructured nickel oxides and their composite electrodes for high-performance supercapacitors," J. Power Sources, **308** (2016): 121-140.
20. L. Zhang, W. Du, A. Nautiyal, Z. Liu, and X. Zhang, "Recent progress on nanostructured conducting polymers and composites: synthesis, application and future aspects," Sci. China Mater., **61** (2018): 303-352.
21. A. Viswanathan, and A.N. Shetty, "Effect of dopants on the energy storage performance of reduced graphene oxide/polyaniline nanocomposite," Electrochim. Acta, **327** (2019): 135026.
22. H.R. PC, A.C. Anbalagan, J. Amalraj, S. Chandrasekaran, and P. Ruz, "Development of surfactant integrated polyaniline based electrode material towards supercapacitor application," Colloids Surf. A: Physicochem. Eng. Asp., **688** (2024): 133545.

23. C. Pan, H. Gu, and L. Dong, "Synthesis and electrochemical performance of polyaniline@ MnO2/graphene ternary composites for electrochemical supercapacitors," J. Power Sources, **303** (2016): 175-181.
24. T. Yonehara, K. Komaba, and H. Goto, "Synthesis of polyaniline in seawater," Polymers, **12** (2020): 375.
25. M. Morshed, J. Wang, M. Gao, C. Cong, and Z. Wang, "Polyaniline and rare earth metal oxide composition: a distinctive design approach for supercapacitor," Electrochim. Acta, **370** (2021): 137714.
26. C. Zhong, Y. Deng, W. Hu, J. Qiao, L. Zhang, and J. Zhang, "A review of electrolyte materials and compositions for electrochemical supercapacitors," Chem. Soc. Rev., **44** (2015): 7484-7539.
27. A. Güngör, F. Bakan-Misirlioglu, G.G. Alturk, and E. Erdem, "Elevating superpacitor performance: Enhancing electrochemical efficiency with transition metal-doped polyaniline electrode. *Journal of Energy Storage*, **76** (2024): 110143.
28. S. Bangning, L. Haijun, Y. Buwei, W. Guanda, L. Hao, S. Hui, and Z. Chun, "Design and construction of low resistance copper doped polyaniline electrode with ultrahigh loading density for high performance supercapacitor applications, Journal of Alloys and Compounds, **964** (2023) 171243.
29. D. Gui, C.Liu, F. Chen, and J. Liu, "Preparation of polyaniline/graphene oxide nanocomposite for the application of supercapacitor. Appl Surf Sci. **307** (2014) 172-177.
30. P. Asen, S. Shahrokhian, and A.I. Zad, "Transition metal ions-doped/grapheme oxide nanostructure as high performance electrode for supercapacitor applications," J Solid State Electrochem. **22** (2018): 983-996.
31. A. Viswanathan, and A.N. Shetty, "Facile in-situ single step chemical synthesis of reducedgraphene oxide-copper oxide-polyaniline nanocomposite and electrochemical performance for supercapacitor application," Electrochim. Acta Theriol. **257**, (2017): 483-493.
32. M.D.A. Khan, A. Akhtar, and S.A. Nabi, "Investigation of the electrical conductivity and optical property of polyaniline-based nanocomposite and its application as an ethanol vapor sensor," N. J. Chem. **39** (2015): 3728–3735.

33. G. Bahmanrokh, C. Cazorla, S.S. Mofarah, R. Shahmiri, Y. Yao, I. Ismail, W.F. Chen, P. Koshy, and C.C. Sorrell, "Band gap engineering of Ce-doped anatase TiO2 through solid solubility mechanisms and new defect equilibria formalism," Nanoscale **12** (2020): 4916–4934.
34. E. A. Sanches , J. C. Soares , A. C. Mafud , E. G. R. Fernandes , F. L. Leite and Y. P. Mascarenhas, "Structural characterization of chloride salt of conducting polyaniline obtained by XRD, SAXD, SAXS and SEM," *J. Mol. Struct.*, **1036** (2013) 121 —126
35. S. Jiang , S. Li , Y. Xu , Z. Liu , S. Weng , M. Lin , Y. Xu , Y. Jiao and J. Chen , "An iron based organic framework coated with nickel hydroxide for energy storage, conversion and detection," *J. Colloid Interface Sci.*, **600** (2021) 150 —160.
36. M.A. Marwat, S. Ishfaq, K.M. Adam, B. Tahir, M.H. Shaikh, M.F. Khan, M.R.A. Karim, Z.U. Din, S. Abdullah, and Ghazanfar, E., "Enhancing supercapacitor performance of Ni–Co–Mn metal–organic frameworks by compositing it with polyaniline and reduced graphene oxide," RSC Adv., **14** (2024): 2102-2115.
37. C. Ren, X. Jia, W. Zhang, D. Hou, Z. Xia, D. Huang, J. Hu, S. Chen, and S. Gao, "Hierarchical porous integrated Co1− xS/CoFe2O4@ rGO nanoflowers fabricated via temperature- controlled in situ calcining sulfurization of multivariate CoFe- MOF- 74@ rGO for high- performance supercapacitor," *Advanced Functional Materials*, **30** (2020): 2004519.
38. R. Ramachandran, Y. Lan , Z.-X. Xu and F. Wang , "Construction of NiCo-layered double hydroxide microspheres from Ni-MOFs for high-performance asymmetric supercapacitors," *ACS Appl. Energy Mater.*, **3** (2020) 6633 —6643.

Figure Captions

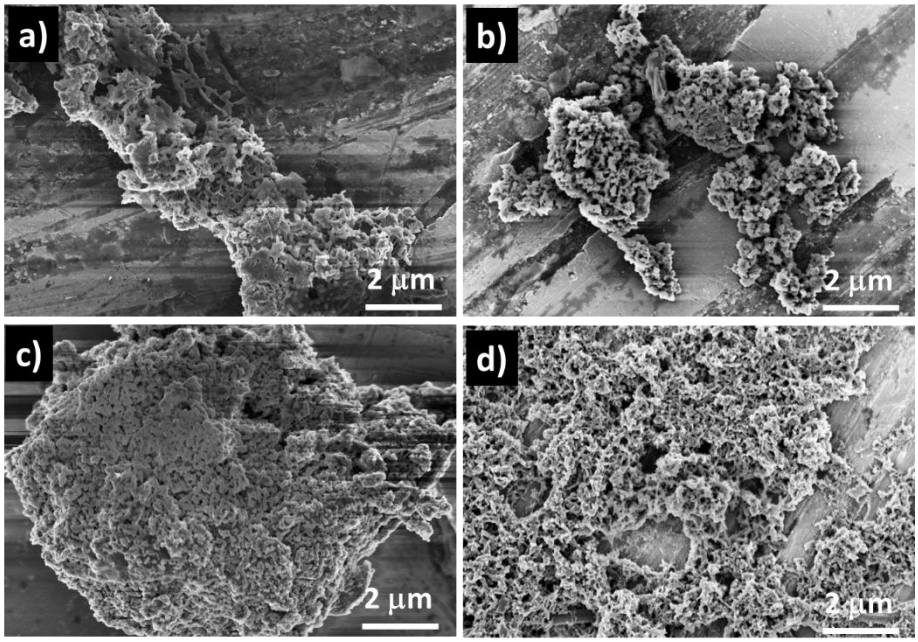

Figure 1: SEM images of a) pure PANI, b) Ag-doped PANI, c) Cu-doped PANI and d) Ag-Cu doped PANI.

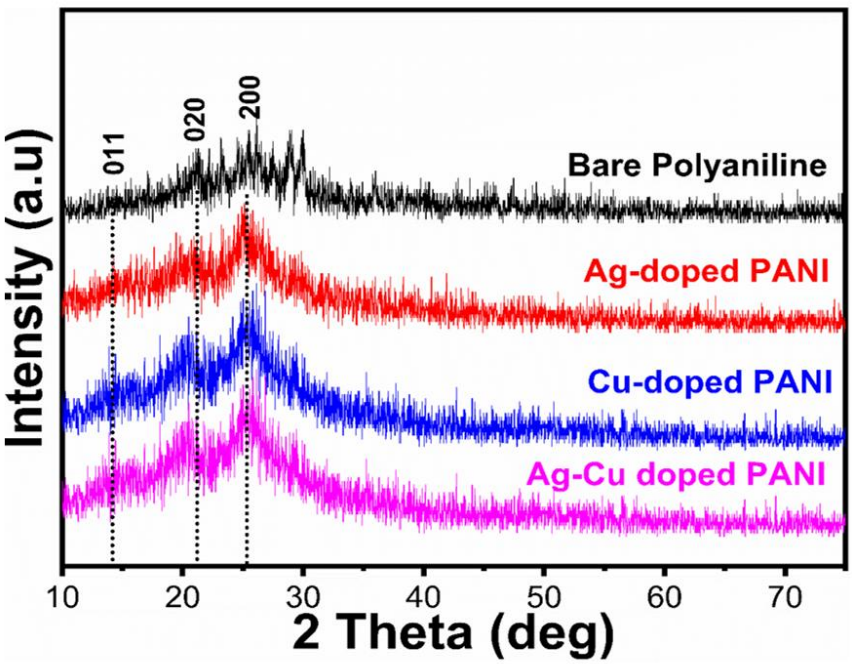

Figure 2: Powder XRD diffraction patterns of bare PANI, Ag doped PANI, Cu doped PANI, and Ag-Cu doped PANI.

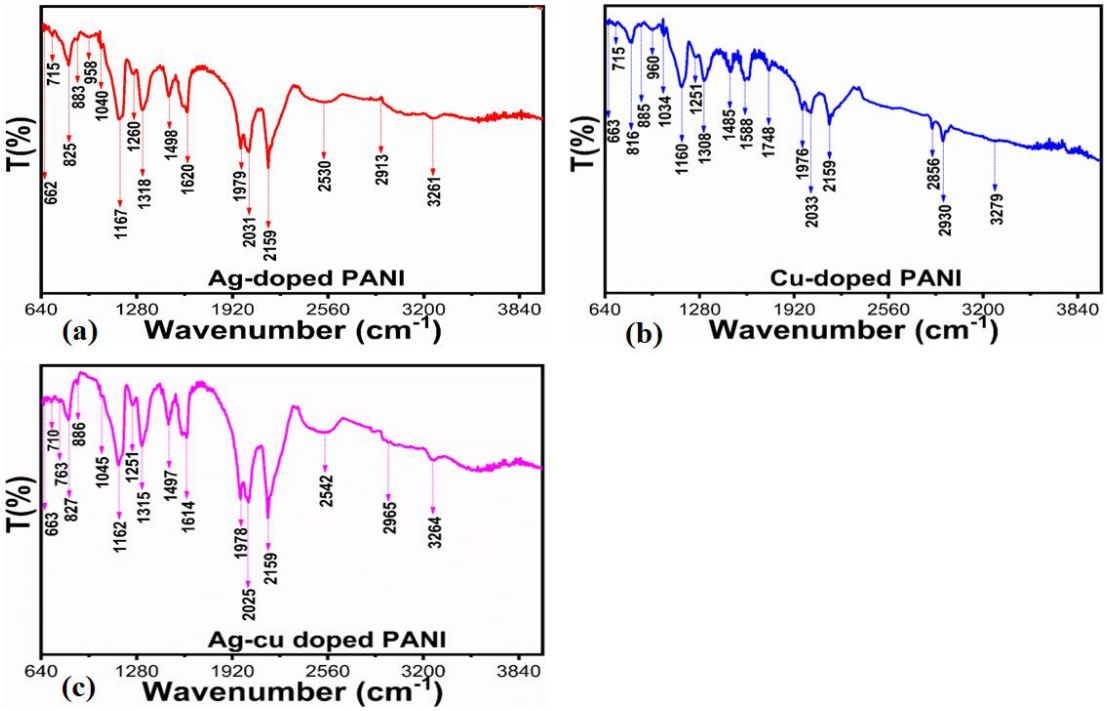

Figure 3: (a-c) FTIR spectra of different materials including Ag doped PANI, Cu doped PANI, and Ag-Cu doped PANI.

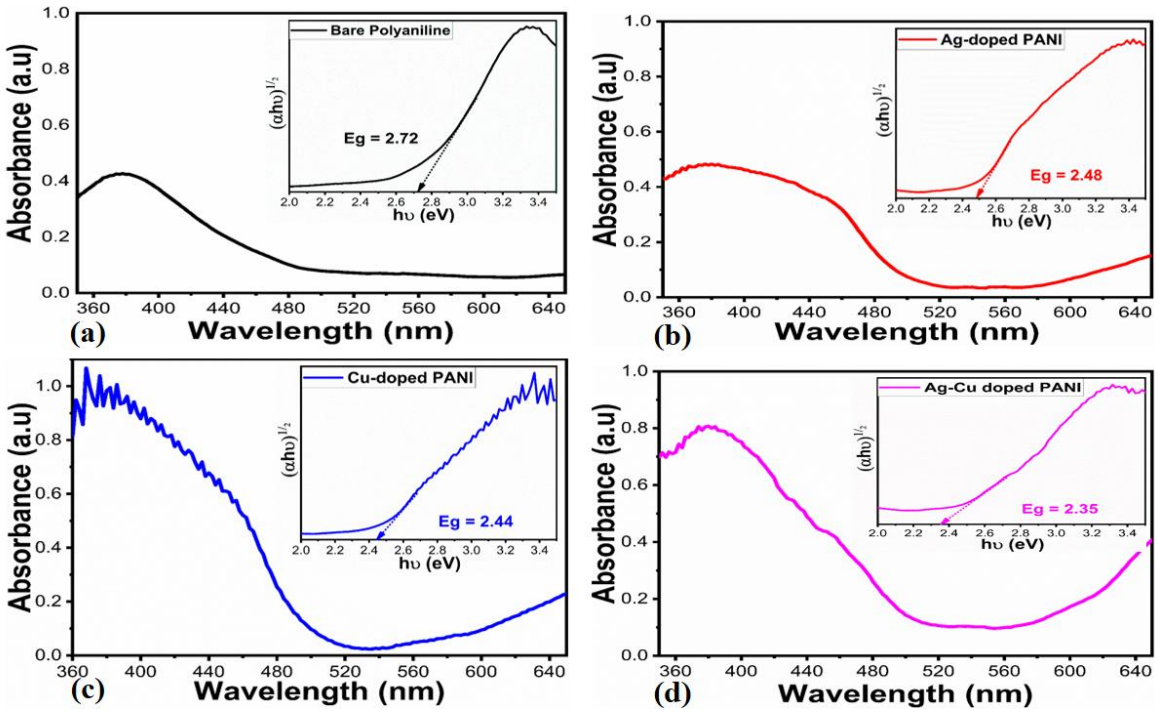

Figure 4: (a-d) UV-visible absorption spectra bare PANI, Ag doped PANI, Cu doped PANI, and Ag-Cu doped PANI, and corresponding inset showing the Tauc plot with estimated optical band gap.

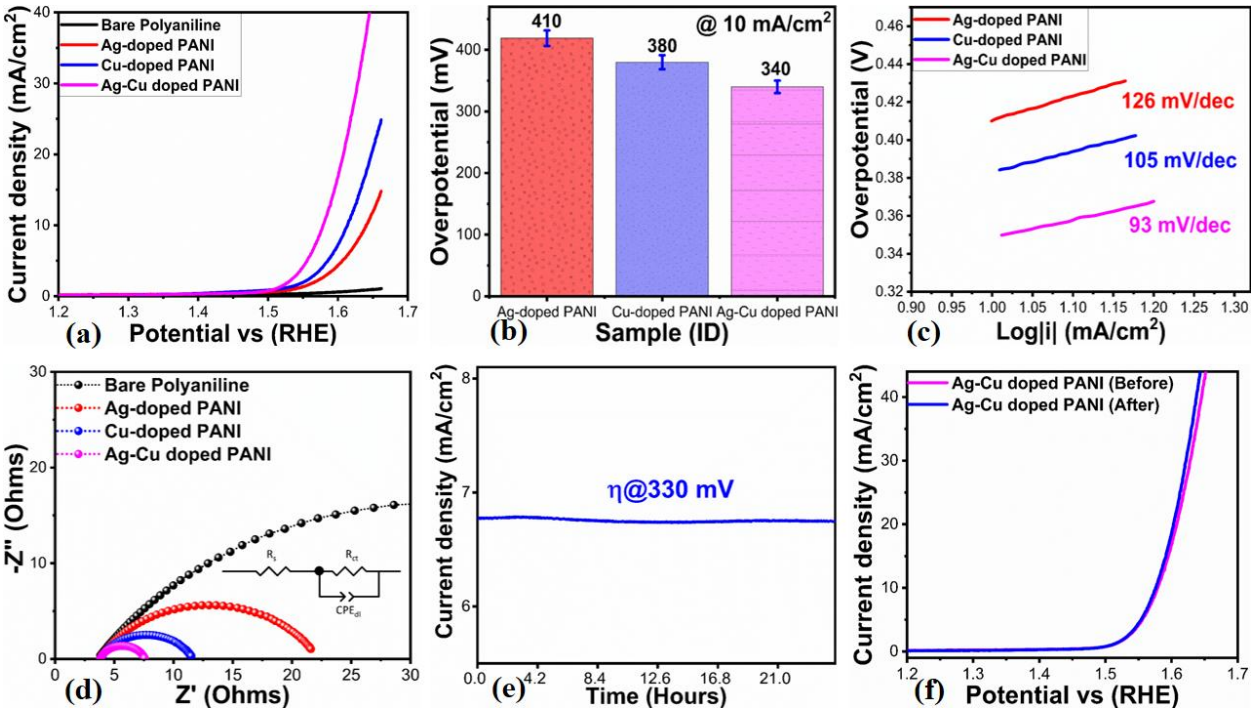

Figure 5: (a) LSV curves for bare PANI, Ag doped PANI, Cu doped PANI, and Ag-Cu doped PANI measured at san rate of 2 mV/s in 1M KOH aqueous solution, (b) Bar graph representation of Ag doped PANI, Cu doped PANI, and Ag-Cu doped PANI, (c) Corresponding Tafel analysis, (d) Nyquist plots of bare PANI, Ag doped PANI, Cu doped PANI, and Ag-Cu doped PANI for exploration of charge transfer resistance, inset shown as fitted equivalent circuit with well-defined circuit elements. (e) Chronoamperometry test for 30 hours at fixed overpotential of 330m mV in 1M KOH solution (f) LSV curves before and after durability test for 30 hours at 2mV/s for the illustrating stability of Ag-Cu doped PANI.

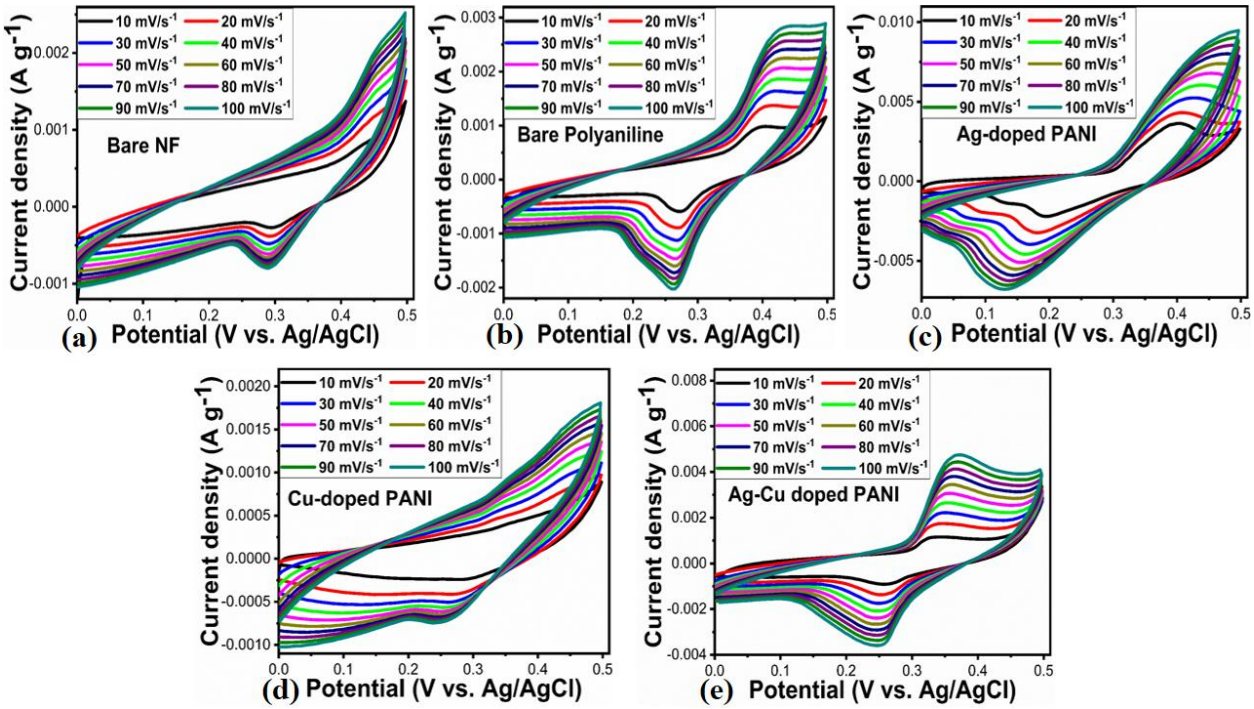

Figure 6: (a-e) CV profiles recorded in 3 M KOH electrolytic solution at different scan rates for bare nickel foam/PANI, Ag doped PANI, Cu doped PANI, and Ag-Cu doped PANI.

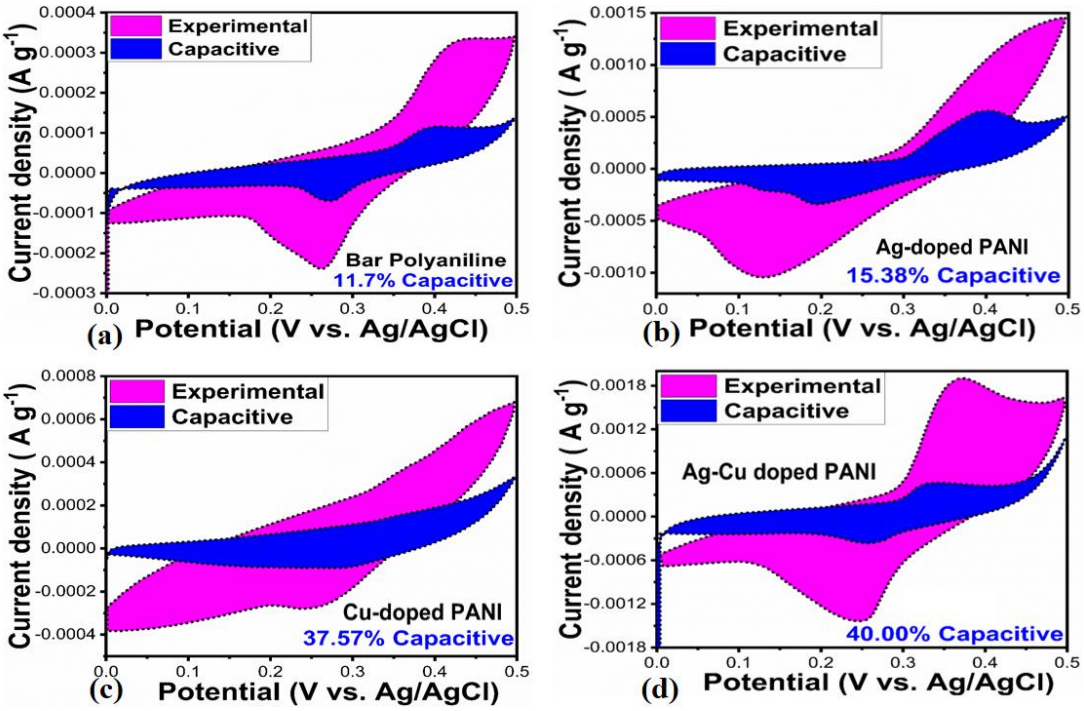

Figure 7: (a-d) Capacitive and diffusion contribution of bare PANI, Ag doped PANI, Cu doped PANI, and Ag-Cu doped PANI at fixed scan rate of 100 mV/s in 3M KOH solution.

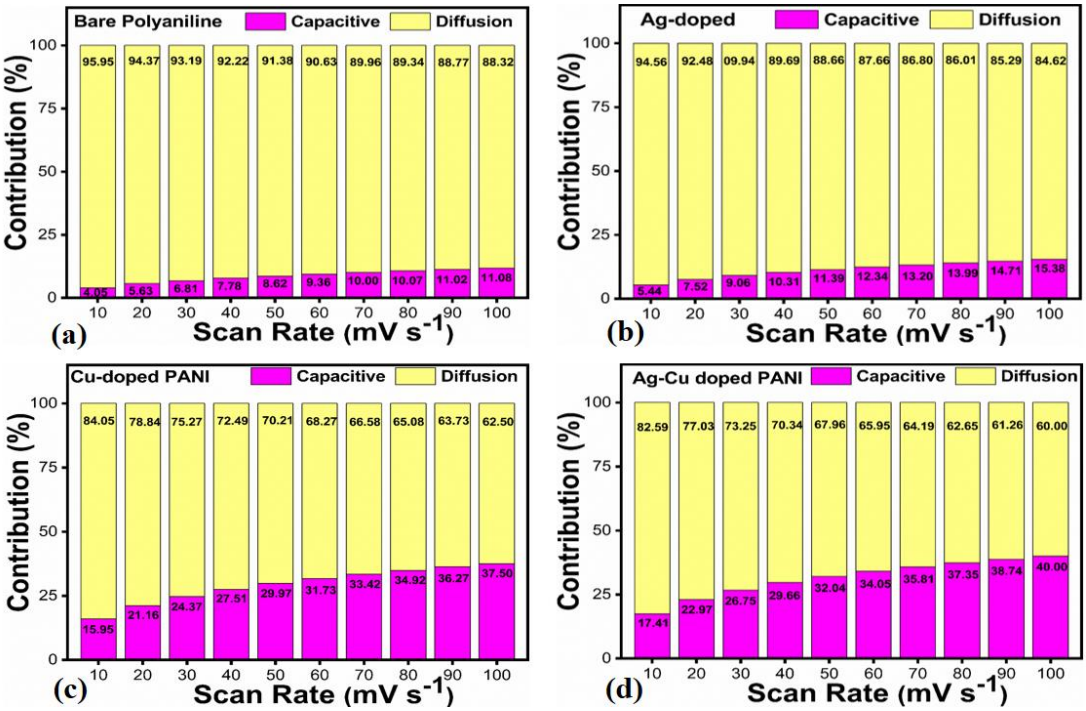

Figure 8: (a-d) Bar graph representation of capacitance and diffusion contribution of bare PANI, Ag doped PANI, Cu doped PANI, and Ag-Cu doped PANI in 3 MKOH solution at various sweeping scan rates.

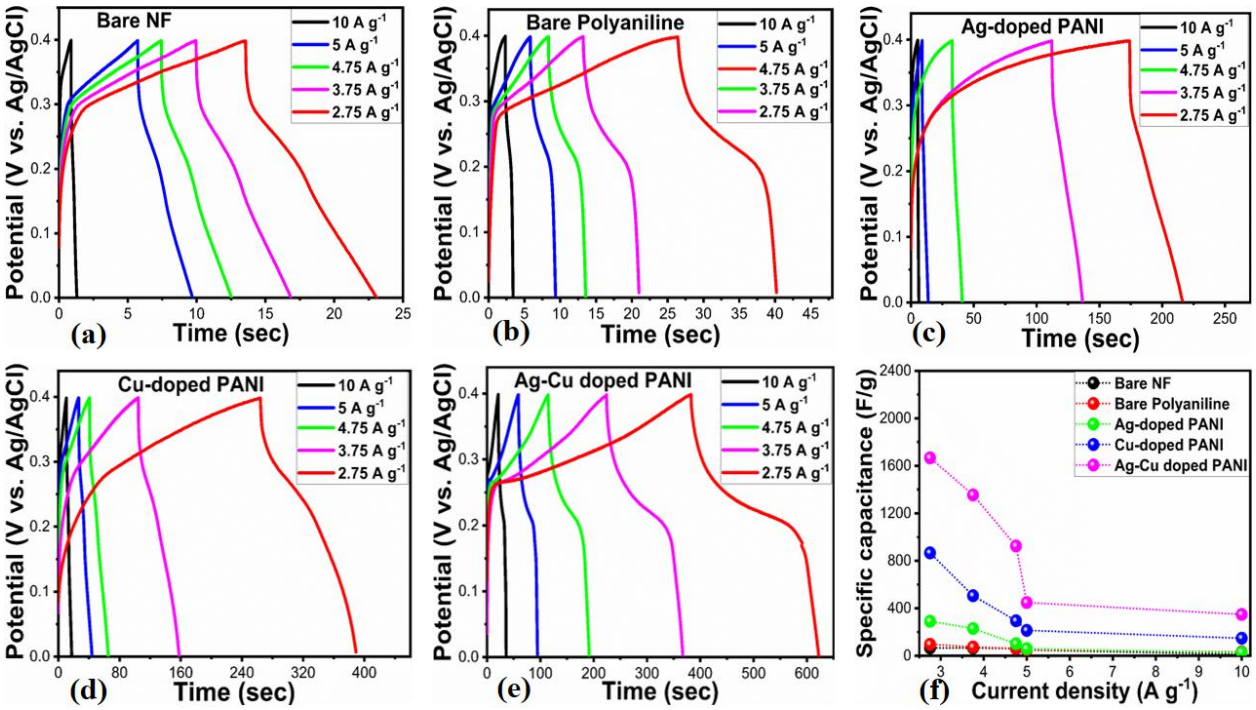

Figure 9: (a-e) GCD curves at different current densities measured for bare nickel foam/PANI, Ag doped PANI, Cu doped PANI, and Ag-Cu doped PANI in 3 M KOH solution, (e) Calculated specific capacitance for each electrode material.

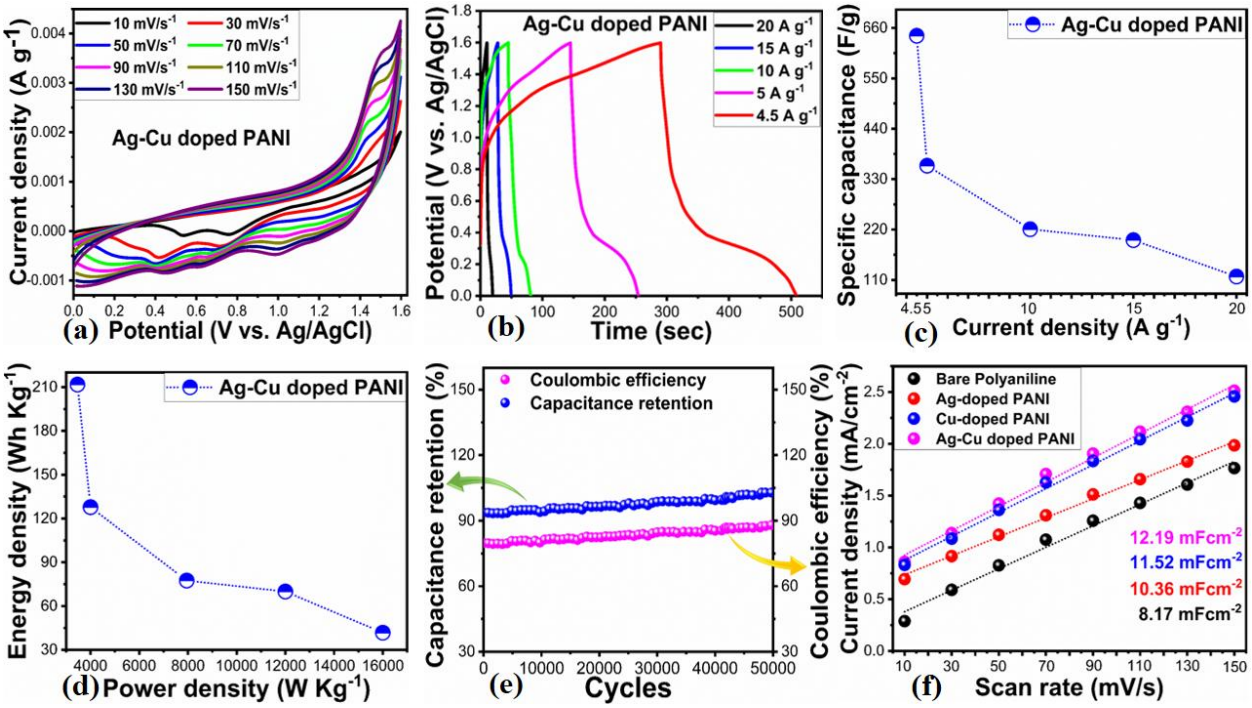

Figure 10: (a) CV curves of Ag-Cu doped PANI at various sweeping scan rate in 3M KOH during configuration of ASC device, (b) Corresponding GCD curves at various current densities, (c) Calculated specific capacitance, (d) Energy and power densities of ASC device, (e) Capacitance retention % and columbic efficiency of ASC, (f) Estimated ECSA values for the bare PANI, Ag doped PANI, Cu doped PANI, and Ag-Cu doped PANI.

Table 1: Brief information about the ASC device demonstration of Ag-Cu doped PANI.

Material	Specific Capacitance (F/g)	Current Density (A/g)	Energy Density (Wh kg^{-1})	Power Density (W kg^{-1})	Columbic efficiency %
Ag-Cu doped PANI	642.86	4.5	211.75	3465.00	87.9%
	359.38	5	127.78	4000.00	
	220.75	10	77.51	7950.00	
	196.88	15	70.00	12000.00	
	117.50	20	41.78	16000.00	

Supplementary information

Utilization of coinage metals as an efficient dopant protocol for enhancing asymmetric supercapacitors and oxygen evolution reactions

Ambedker[a], Ahmed Raza[a], Haresh Kumar[a], Jethanand[a], Wanhinyal[a], Rameez Mangi[a], Masroor Ali Bhellar[a], Fida Hussain[a], Ghansham Das[a], Kashif Ali[a], Aneela Tahira[c], Muhammad Ali Bhatti[f], Elmuez Dawi[d], Rafat M. Ibrahim[e], Brigitte Vigolo[b], Jawaid Ali Lighari[f], Zafar Hussain Ibupoto[a*]

[a]*Institute of Chemistry, University of Sindh Jamshoro, 76080, Sindh, Pakistan.*

[b]*University de Lorraine, CNRS, IJL, F-54000 Nancy, France.*

[c]*Institute of Chemistry, Shah Abdul Latif University Khairpur Mirs, Sindh, Pakistan.*

[d]*College of Humanities and Sciences, Mathematics and Science department, Ajman University, P.O.Box 346, Ajman, UAE.*

[e]*Physics Department, Faculty of Science, Taibah University, Al- Madaina Al Munawarah 42353, Saudi Arabia*

[f]*Centre for Environmental Sciences, University of Sindh Jamshoro, 76080, Sindh, Pakistan.*

[*]*Corresponding author(s):*

Zafar Hussain Ibupoto, PhD, Email : zaffar.ibhupoto@usindh.edu.pk

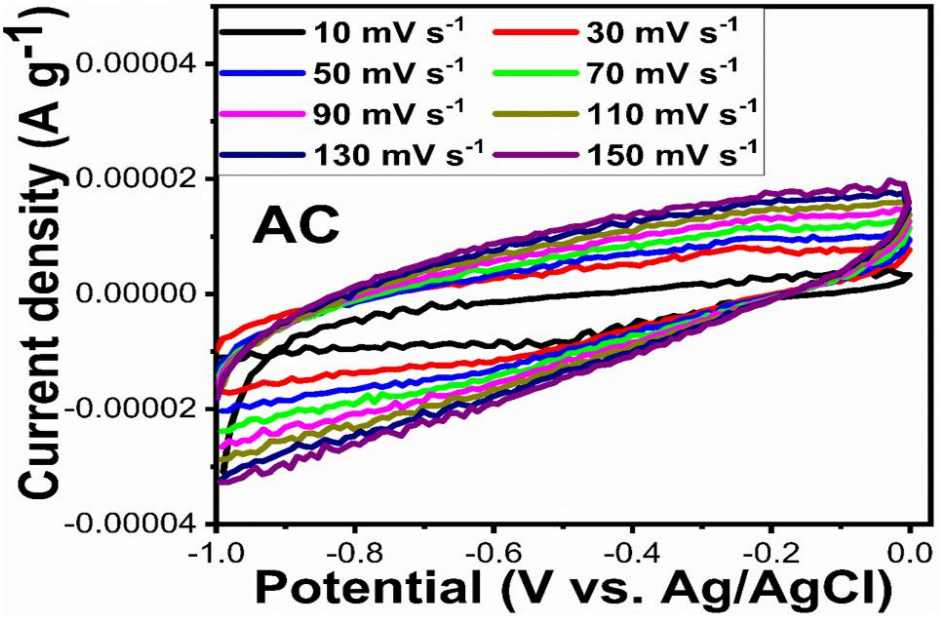

Figure (S1): CV profiles of AC at different scan rates in 3 M KOH solution.

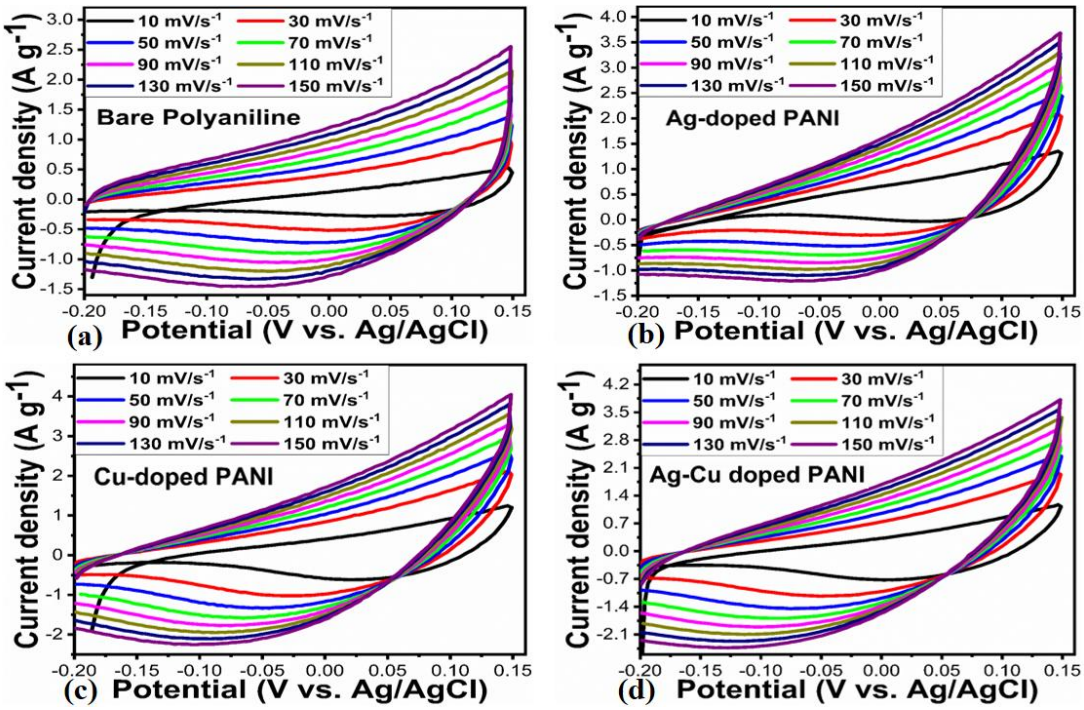

Figure (S2a-d): Non-faradic CV curves of bare PANI, Ag doped PANI, Cu doped PANI, and Ag-Cu doped PANI At various scan rates in 3M KOH electrolytic solution.

Table (S1). A comparative study with other already reported results.

Material	**Tafel slope (mV/dec)**	**Overpotential (mV)**	**Current density ($mA\ cm^{-2}$)**	Reference
NiO/MnO_2@PANI	24	345	10	1
CoPO	60.7	350	10	2
Co/b-Mo_2C@N-CNTs	67	356	10	3
$NiCo_2O_4$/PANI	153	400	10	4
CuCoS/PANI	55	200	10	5
$Fe_{90}Nb_{10}$	50	340	10	6
$Co_{2.25}Fe_{0.75}O_4$	50	350	10	7
NiFeG	74	320	10	8
Ni0.25Cu0.75/C	80	400	10	9
Ni0.25Co0.75 (OH)2	71	352	10	10
Pr/Nd co-doped CeO_2	84	274	10	11
(Sm)-doped $NiMnO_3$	109	321	10	12
Ag-Cu	**93**	**340**	**10**	**Here in**

1. J. He, M. Wang, W. Wang, R. Miao, W. Zhong, S.Y. Chen, S. Poges, T. Jafari, W. Song, J. Liu, and S.L. Suib, "Hierarchical mesoporous NiO/MnO2@ PANI core–shell microspheres, highly efficient and stable bifunctional electrocatalysts for oxygen evolution and reduction reactions," ACS Appl Mater Interfaces. **9** (2017): 42676–42687.
2. P. Bhanja, Y. Kim, B. Paul, J. Lin, S. M. Alshehri, T. Ahamad, Y. V. Kaneti, A. Bhaumik and Y. Yamauchi, "Facile synthesis of nanoporous transition metal- based phosphates for oxygen evolution reaction," *ChemCatChem* **12** (2020): 2091-2096.
3. T. Ouyang, Y.-Q. Ye, C.-Y. Wu, K. Xiao, Z.-Q. Liu, "Heterostructures Composed of N-Doped Carbon Nanotubes Encapsulating Cobalt and β-Mo2C Nanoparticles as

Bifunctional Electrodes for Water Splitting," Angewandte Chemie International Edition, **58** (2019): 4923-4928.

4. M. Bhushan, M. Mani, A.K. Singh, A.B. Panda, and V.K. Shahi, "Self-standing polyaniline membrane containing quaternary ammonium groups loaded with hollow spherical NiCo2O4 electrocatalyst for alkaline water electrolyser," Journal of Materials Chemistry A, **8** (2020): 17089-17097.
5. H. Hassan, M.W. Iqbal, H. Alrobei, F. Riasat, A.M. Afzal, A.M. Saeedi, H.B. Albargi, and A. Rehmat, "Synergistic CuCoS–PANI materials for binder-free electrodes in asymmetric supercapacitors and oxygen evolution," *Nanoscale Advances*, *6* (2024): 1507-1523.
6. C. Wang, R. Wang, Y. Peng, J. Chen, Z. Chen, H. Yin, and J. Li, "Nb-incorporated Fe (oxy)hydroxide derived from structural transformation for efficient oxygen evolution electrocatalysis," Journal of Materials Chemistry A, **8** (2020): 24598-24607.
7. S. Saddeler, G. Bendt, S. Salamon, F.T. Haase, J. Landers, J. Timoshenko, C. Rettenmaier, H.S. Jeon, A. Bergmann, H. Wende, B. Roldan Cuenya, and S. Schulz, "Influence of the cobalt content in cobalt iron oxides on the electrocatalytic OER activity," Journal of Materials Chemistry A, ***9*** (2021): 25381-25390.
8. V.K. Singh, B. Malik, R. Konar, E.S. Avraham, and G.D. Nessim, The Electrocatalytic Oxygen Evolution Reaction Activity of Rationally Designed NiFe-Based Glycerates. *Electrochem*, ***5*** (2024.) 70-83.
9. M.A. Ahsan, A.R. Puente Santiago, Y. Hong, N. Zhang, M. Cano, . Rodriguez-Castellon, L. Echegoyen, S.T. Sreenivasan, and J.C. Noveron, Tuning of trifunctional NiCu bimetallic nanoparticles confined in a porous carbon network with surface composition and local structural distortions for the electrocatalytic oxygen reduction, oxygen and hydrogen evolution reactions. *Journal of the American Chemical Society*, ***142*** (2020) 14688-14701.
10. Y. Wang, C. Yang, Y. Huang, Z. Li, Z. Liang, and G. Cao, Nickel induced electronic structural regulation of cobalt hydroxide for enhanced water oxidation. *Journal of Materials Chemistry A, **8*** (2020) 6699-6708.
11. T. Munawar, A. Bashir, M.U. Nisa, R.A. Alshgari, F. Mukhtar, S. Mohammad, M.N. Ashiq, M.F. Ehsan, F. Iqbal, and S.I. Allakhverdiev, Unravelling the operando structural

and chemical stability of rare earth metals co-doped CeO2-based electrocatalysts for oxygen evolution reaction. *International Journal of Hydrogen Energy*. (2024)

12. S. Swathi, R. Yuvakkumar, G. Ravi, A.G. Al-Sehemi, and D. Velauthapillai, Rare earth metal (Sm)-doped NiMnO 3 nanostructures for highly competent alkaline oxygen evolution reaction. *Nanoscale Advances*, ***4*** (2022) 2501-2508.

Table (S2): Summarized supercapacitor performance of bare nickel foam and PANI, Ag doped PANI, Cu doped PANI, and Ag-Cu doped PANI.

Material	Specific Capacitance (F/g)	Current Density (A/g)
Bare NF	66.50	2.75
	65.01	3.75
	59.67	4.75
	48.87	5
	12.53	10
Bare PANI	96.28	2.75
	74.43	3.75
	62.06	4.75
	51.38	5
	32.58	10
Ag-doped PANI	290.93	2.75

	229.90	3.75
	101.44	4.75
	60.15	5
	27.57	10
Cu-doped PANI	866.56	2.75
	505.97	3.75
	294.79	4.75
	213.57	5
	147.87	10
Ag-Cu doped PANI	1667.32	2.75
	1354.90	3.75
	924.94	4.75
	448.62	5
	348.37	10

Table (S3). The asymmetrical device performance of supercapacitors.

Material	Specific Capacitance (F/g)	Energy Density (Wh kg^{-1})	Power Density (W kg^{-1})	Operating Voltage window	Reference
rGO/Fe_3O_4/PANI	283.4	47.7 W h kg^{-1}	550	1.6 V	1

$NiCu(OH)_2CO_3$//AC	476 F g^{-1}	48.55 Wh kg^{-1}	541 W kg^{-1}	0.6 V	2
RuO_2//h-WO_3	47.59 F g^{-1}	16.92 W h kg^{-1}	540 W/kg	1.6 V	3
Co1Ni1//AC	106	42.5 Wh kg^{-1}	849.7 W k g^{-1}	1.7 V	4
MnO_2/HCS-30//HCS	74.5 F g^{-1}	41.4 Wh kg^{-1}	-------	2.0 V	5
$NiCo_2O_4$@MnO_2 //AC	112 F g^{-1}	58.9 W h kg^{-1}	400 W kg^{-1}	1.5 V	6
$MnCo_2O_{4.5}$-40 GQDs//rGO Ag QDs/	200 F g^{-1}	46 Wh kg^{-1}	66 W kg^{-1}	1.3 V	7
$NiMoO_4$//spore-derived AC	120.5 F g^{-1}	48.5 Wh kg^{-1}	212.5 kWh kg^{-1}	1.7 V	8
ZnO@CoS//AC	2438 mC cm^{-2}	45.2 Wh kg^{-1}	1039.1 W kg^{-1}	1.6V	9
$CoMoO_4$@CoS//AC	189.5 F g^{-1}	59.2 W h kg^{-1}	799.8 W k g^{-1}	1.7 V	10
NiCo–CH-180//AC	125	52	1500 W kg^{-1}	1.7 V	11
Ag-Cu	**642.86**	**211.75**	**3465.00**	**1.6V**	**Here in**

1. S. Mondal, U. Rana, and S. Malik, "Reduced graphene oxide/Fe3O4/polyaniline nanostructures as electrode materials for an all-solid-state hybrid supercapacitor," *The Journal of Physical Chemistry C*, ***121*** (2017): 7573-7583.
2. X. Zheng, Y. Ye, Q. Yang, B. Geng, and X. Zhang, "Ultrafine Nickel-Copper Carbonate Hydroxide Hierarchical Nanowire Networks for High-Performance Supercapacitor Electrodes," *Chem. Eng. J.*, **290** (2016): 353–360.
3. S.H. Ji, N.R. Chodankar, and D.H. Kim, Aqueous asymmetric supercapacitor based on RuO2-WO3 electrodes. *Electrochimica Acta*, ***325*** (2019): 134879.
4. X.-L. Wang, G.-F. Zhang, R. Nasser, T.-T. Jiang, Q.-W. Cao, M. Gong, X.-Y. Li, and J.-M. Song, "Controllable Synthesis of Co/Ni Basic Carbonate Composite *via* Regulating Co/Ni Ratio with Super Rate Performance for Asymmetric Solid-state Supercapacitor," *J. Alloys Compd.*, **906** (2022) 164270.

5. W. Du, X. Wang, J. Zhan, X. Sun, L. Kang, F. Jiang, X. Zhang, Q. Shao, M. Dong, H. Liu, and V. Murugadoss, "Biological cell template synthesis of nitrogen-doped porous hollow carbon spheres/MnO2 composites for high-performance asymmetric supercapacitors," *Electrochimica Acta*, ***296*** (2019): 907-915.
6. D. Zhu, X. Sun, J. Yu, Q. Liu, J. Liu, R. Chen, H. Zhang, R. Li, J. Yu, and J. Wang, "Rationally designed CuCo2O4@ Ni (OH) 2 with 3D hierarchical core-shell structure for flexible energy storage," *Journal of colloid and interface science*, ***557*** (2019) 76-83.
7. M. Zhang, W. Liu, R. Liang, R. Tjandra, and A. Yu, "Graphene quantum dot induced tunable growth of nanostructured MnCo 2 O 4.5 composites for high-performance supercapacitors," *Sustainable Energy & Fuels*, ***3*** (2019): 2499-2508.
8. X. Zhang, Z. Li, Z. Yu, L. Wei, and X. Guo, „Mesoporous NiMoO4 microspheres decorated by Ag quantum dots as cathode material for asymmetric supercapacitors: enhanced interfacial conductivity and capacitive storage," *Applied Surface Science*, ***505*** (2020): 144513.
9. S. Ding, X. Li, X. Jiang, Q. Hu, Y. Yan, Q. Zheng, and D. Lin, "Core-shell nanostructured ZnO@ CoS arrays as advanced electrode materials for high-performance supercapacitors," *Electrochimica Acta*, ***354*** (2020): 136711.
10. H. Xuan, H. Li, J. Yang, X. Liang, Z. Xie, P. Han, and Y. Wu, Rational design of hierarchical core-shell structured CoMoO4@ CoS composites on reduced graphene oxide for supercapacitors with enhanced electrochemical performance. *International Journal of Hydrogen Energy*, *45* (2020): 6024-6035.
11. S. Kumar, B.K. Satpathy, and D. Pradhan, Morphology-controlled synthesis of a NiCo-carbonate layered double hydroxide as an electrode material for solid-state asymmetric supercapacitors. *Materials Advances*, ***5*** (2024): 2271-2284.